Significance Of Nuclear Quantum Effects In Hydrogen Bonded Molecular Chains

Aleš Cahlík, Jack Hellerstedt, Jesús I Mendieta-Moreno, Martin Švec, Vijai M Santhini, Simon Pascal, Diego Soler-Polo, Sigurdur Erlingsson, Karel Výborný, Pingo Mutombo, et al.

Significance Of Nuclear Quantum Effects In Hydrogen Bonded Molecular Chains

Aleš Cahlík[1,2,3†], Jack Hellerstedt[1†], Jesús I. Mendieta-Moreno[1†], Martin Švec[1,3], Vijai M. Santhini[1,3], Simon Pascal[4], Diego Soler-Polo[5], Sigurdur Erlingsson[6], Karel Výborný[1], Pingo Mutombo[1,8], Ondrej Marsalek[7], Olivier Siri[4]*, Pavel Jelínek[1,3]*

[1] Institute of Physics of the Czech Academy of Sciences, v.v.i., Cukrovarnicka 10, CZ-16200 Prague 6, Czech Republic

[2] Faculty of Nuclear Sciences and Physical Engineering, Czech Technical University in Prague, Břehová 78/7, CZ-11519 Prague 1, Czech Republic

[3] Regional Centre of Advanced Technologies and Materials, Palacký University, Šlechtitelů 27, CZ-78371 Olomouc, Czech Republic

[4] Aix Marseille Univ, CNRS, CINaM, UMR 7325, Campus de Luminy, F-13288 Marseille Cedex 09, France

[5] Universidad Autónoma de Madrid, Campus Cantoblanco, ES-28049, Madrid, Spain

[6] School of Science and Engineering, Reykjavik University, Menntavegi 1, IS-101 Reykjavik, Iceland

[7] Charles University, Faculty of Mathematics and Physics, Ke Karlovu 3, CZ-12116 Prague 2, Czech Republic

[8] Department of Petrochemistry and Refining, University of Kinshasa, Kinshasa, Democratic Republic of Congo

ABSTRACT: In hydrogen bonded systems, nuclear quantum effects such as zero-point motion and tunneling can significantly affect their material properties through underlying physical and chemical processes. Presently, direct observation of the influence of nuclear quantum effects on the strength of hydrogen bonds with resulting structural and electronic implications remains elusive, leaving opportunities for deeper understanding to harness their fascinating properties. We studied hydrogen-bonded one-dimensional quinonediimine molecular networks which may adopt two isomeric electronic configurations *via* proton transfer. Herein, we demonstrate that concerted proton transfer promotes a delocalization of π-electrons along the molecular chain, which enhances the cohesive energy between molecular units, increasing the mechanical stability of the chain and giving rise to distinctive electronic in-gap states localized at the ends. These findings demonstrate the identification of a class of isomeric hydrogen bonded molecular systems where nuclear quantum effects play a dominant role in establishing their chemical and physical properties. This identification is a step towards the control of mechanical and electronic properties of low-dimensional molecular materials *via* concerted proton tunneling.

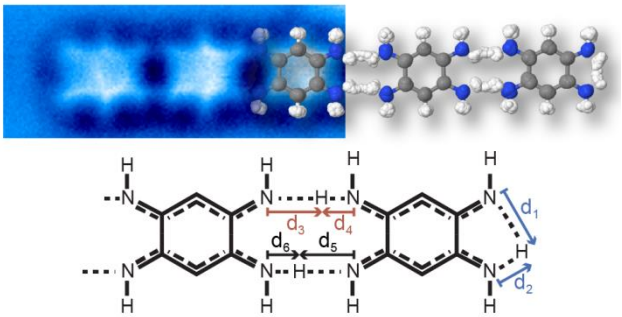

KEYWORDS: nuclear quantum effects, scanning probe microscopy, proton tunneling, hydrogen bonds, path integral molecular dynamics, in-gap electronic states, π-electron delocalization

Nuclear quantum effects (NQEs), such as proton tunneling and zero-point motion can play an important role in understanding structural[1] and material properties[2–4] of hydrogen-bonded systems at low temperatures. It has been demonstrated both theoretically[5] and experimentally[6] that nuclear quantum effects may have a pronounced two-fold effect on the strength of hydrogen bonds, either further weakening of already weak hydrogen bonds or conversely, strengthening of the relatively strong ones. NQEs can induce strong proton delocalization with direct consequences on chemical activity of the system.[7] Complex, concerted many-body proton motion in ice has been described both experimentally[8] and theoretically.[9,10] Proton transfer processes have also been also studied by scanning tunneling microscopy.[11-15] In this context, recent progress in scanning probe microscopy providing spatial resolution on single molecules *via* a proper tip functionalization[16,17] has enabled the direct observation of concerted proton motion in water tetramers.[18]

Despite these advances, our present understanding of NQEs remains incomplete. In this work, we show that the concerted proton motion in a H-bonded 1D molecular system not only

enhances its mechanical stability but directly modifies its electronic structure, forming distinct electronic states in the band gap (hereinafter referred as "in-gap states") localized at the ends of the chain.

2,5-diamino-1,4-benzoquinonediimines (DABQDI, structure in Fig.1a inset) belong to a family of quinoid molecules with intriguing electronic properties[19] stemming from a prominent distribution of their π-electrons. DABQDI quinones contain 12 π-electrons which can be perceived as two independent π -subsystems containing 6 conjugated π-electrons (the nitrogen lone pair is conjugated with the two double bonds), chemically linked *via* two C-C σ-bonds, but electronically not conjugated.[20,21] The molecular DABQDI building blocks exist in solution as two tautomers in equilibrium, whose mutual alternation can be realized *via* a fast intramolecular double proton transfer that generates a structure of higher symmetry (*i.e.* an averaged form of the two tautomers) which directly alters the π-conjugation of the whole DABQDI molecule.[17] Curiously, although unsubstituted DABQDI (N-H) was reported in the literature in 1887,[22] this molecule has since rarely been investigated, probably due to its very low solubility and poor stability (co-condensation, hydrolysis, and oxidation side reactions).[23]

Results and discussion

Here we explore self-assembled molecular chains built from the precursor DABQDI on a metallic Au(111) surface at low temperatures (5 K) under ultra-high vacuum conditions. The presence of imine (as H-acceptor) and amine groups (as H-donor) enables, in principle, the formation of 1D intermolecular hydrogen-bonded assemblies. Such chains may adopt two isomeric π-conjugations resulting from the distinct alternation of double and single bonds according to the position of the amine group hydrogen atoms. In principle, the energy landscape of the system can be mimicked by a symmetric double-well potential, which has different ground states in either the classical or quantum picture. While in the classical picture the system is localized in one of the wells, the quantum ground state exists as a superposition of two states.[24] As we will show later on, the quantum state strongly affects the electronic structure of the chain. In this one-dimensional configuration, the presence of concerted proton transfer not only induces resonant tunneling between the two degenerate π-conjugated electronic states of the chain, but it also mediates an effective coupling of the π-electron systems across the chain. This coupling of resonant electronic configurations leads to the emergence of distinct electronic states and reinforcement of the mechanical stability of the molecular chain.

Figure 1a shows a representative overview scanning tunneling microscopy (STM) image acquired at 5 K of linear self-assembled 1D molecular structures. The chains form upon deposition of single DABQDI molecules onto a Au(111) substrate held at low temperature (5 K, AFM image of single DABQDI shown in Supplementary Fig. 1c) which is subsequently warmed to room temperature where the chains self-assemble *via* surface diffusion (for detailed description of the sample preparation see the Experimental Section and Supplementary Information).

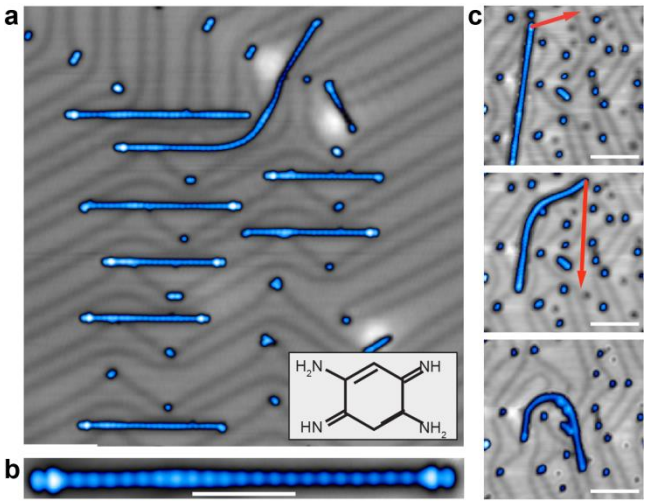

Figure 1: a) Representative overview STM image of molecular chains and single molecule species. (50 mV, 10 pA, scale bar 10nm). Inset: 2,5-diamino-1,4-benzoquinonediimine (DABQDI) structure. b) Close-up STM image of the symmetric chain with characteristic bright spots at the ends. (30 mV, 5 pA, scale bar 5 nm) c) From top to bottom: sequentially acquired STM images of chain manipulation experiment. Red arrows represent the probe movement after contacting the chain end (procedure detailed in Methods) (all images 100 mV, 10 pA, scale bars 10 nm).

Typically, we observe chains with lengths ranging between 3 and 100 nm, oriented independently of the surface herringbone reconstruction. The hallmark of these molecular chains is the presence of characteristic bright spots in STM images located at the ends of the chains, as can be seen in Fig. 1b. In addition to the chains, distinct individual molecular species are present on the substrate, predominantly situated on the herringbone elbows, which we identify as individual molecules containing an extra proton as will be discussed later.

We are readily able to contact and manipulate complete chains along the surface by approaching the tip to a chain end with a subsequent lateral tip movement. Figure 1c displays a series of STM images of the same chain acquired between consecutive manipulations (see also Supplementary Video 1). Chains always remained intact during manipulation without loss of their structural integrity while preserving the bright spots at their ends (Supplementary Fig. 2). This demonstrates not only a weak dispersive interaction between the molecular chains and the underlying metallic surface, but more importantly a relatively strong intermolecular binding.

The picture can qualitatively change when the DABQDI molecules are sublimed onto the surface at room temperature and subsequently cooled down to 5 K for imaging. For certain preparation conditions the resulting molecular chains incorporate more defects, their growth is restricted by the herringbone reconstruction of the Au(111) surface and they lack bright end terminations, as can be seen in Figure 2a. Moreover, the mechanical stability is drastically reduced, making lateral manipulation impossible. Instead, mechanical interaction with the scanning probe easily splits the chains into segments, as shown

in Figure 2b. One possibility to explain the difference in mechanical properties between the two chain types is the impact of proton tunneling on the strength of intramolecular hydrogen bonding. Indeed, the fact that NQEs may further enhance cohesion of relatively strong hydrogen bonds has been explored theoretically,[5,6] but direct observations are lacking. For clarity, in the rest of the manuscript we will refer to the exemplary former species as symmetric chains while the latter will be referred to as canted chains (n.b. experimental control of the formation of symmetric *vs*. canted chains is imperfect: see Methods and extended discussion in the Supplementary Information).

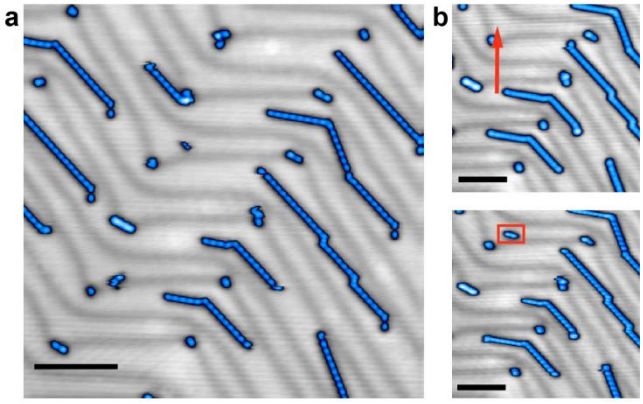

Figure 2: a) Representative overview STM image of canted molecular chains. (140 mV, 20 pA, scale bar 10 nm) b) STM images (140 mV, 20 pA) taken before and after manipulation experiment. Red arrows represent the probe movement after contacting the chain end (procedure detailed in Methods). Image on the right side (after the manipulation) show apparent splitting of the chain into segments. Scale bars 10 nm.

To better understand the internal structure of the adsorbed chains and single molecular species, we acquired high-resolution atomic force microscopy (AFM) images with a CO-functionalized probe.[16,17] This scanning probe technique has repeatedly demonstrated the capabilities of unambiguous discrimination of chemical[25,26] and atomic[27] structure, electrostatic potential mapping,[28] or identification of the spin state[29] of single molecules on surfaces.

The high-resolution AFM image of a single molecular species, not participating in the chain formation, shown in Fig. 3a, reveals a characteristic trapezoidal shape. Perfect agreement of the experimental AFM image with the simulation based on the chemical structure shown in Fig. 3b can be achieved by including the presence of an extra hydrogen in the single molecule species (Fig. 3c, d). The detailed structure of the hydrogenated molecule as well as the origin of the extra hydrogen are discussed in the Supplementary Information. We presume this additional hydrogen impedes an efficient self-assembling process *via* hydrogen bonding with the remaining molecules (the H acceptor capability is suppressed). Figure 3e presents high resolution AFM images of the symmetric chain interior. By registering the molecular structure with the underlying Au(111) surface (see Supplementary Fig. 3) we determined an incommensurable alignment of the molecular chains with the substrate and the distance between two contiguous molecules to be 8.0 ± 0.1 Å. This excludes the possibility of covalent bonding between nitrogen atoms, since the Density Functional Theory (DFT) calculated periodicity of a chain composed of covalently bonded molecules is significantly lower (5.7 Å, see Supplementary Fig. 4e). The fact that our experiments are carried out in UHV conditions significantly reduces the possibility of contamination. A natural explanation of the large mechanical stability of symmetric chains would be a formation of organometallic chains with gold adatoms. However, this scenario can be ruled out by several observations. Namely, XPS measurements of DABQDI molecules deposited on Au(111) at room temperature show in N1s region two distinct components corresponding to both -NH2 and –NH groups (see Figure S3 in Santhini *et al.*[30]). Moreover, in very rare instances we observe the formation of short defective chains (see Supplementary Fig. 4a), whose AFM contrast is clearly distinct from the straight chain since it shows a characteristic “x-like” feature in between the molecular units. Such contrast feature fits well to simulated AFM images of a fully optimized metal-organic Au-DABQDI chain with four-fold coordinated gold atoms on a Au(111) surface obtained from total energy DFT calculations (Supplementary Fig. 4b, c). More elaborate discussion ruling out the presence of the gold organometallic chains and the other possible scenario, the gain or loss of additional hydrogens, can be found in the Supplementary Information.

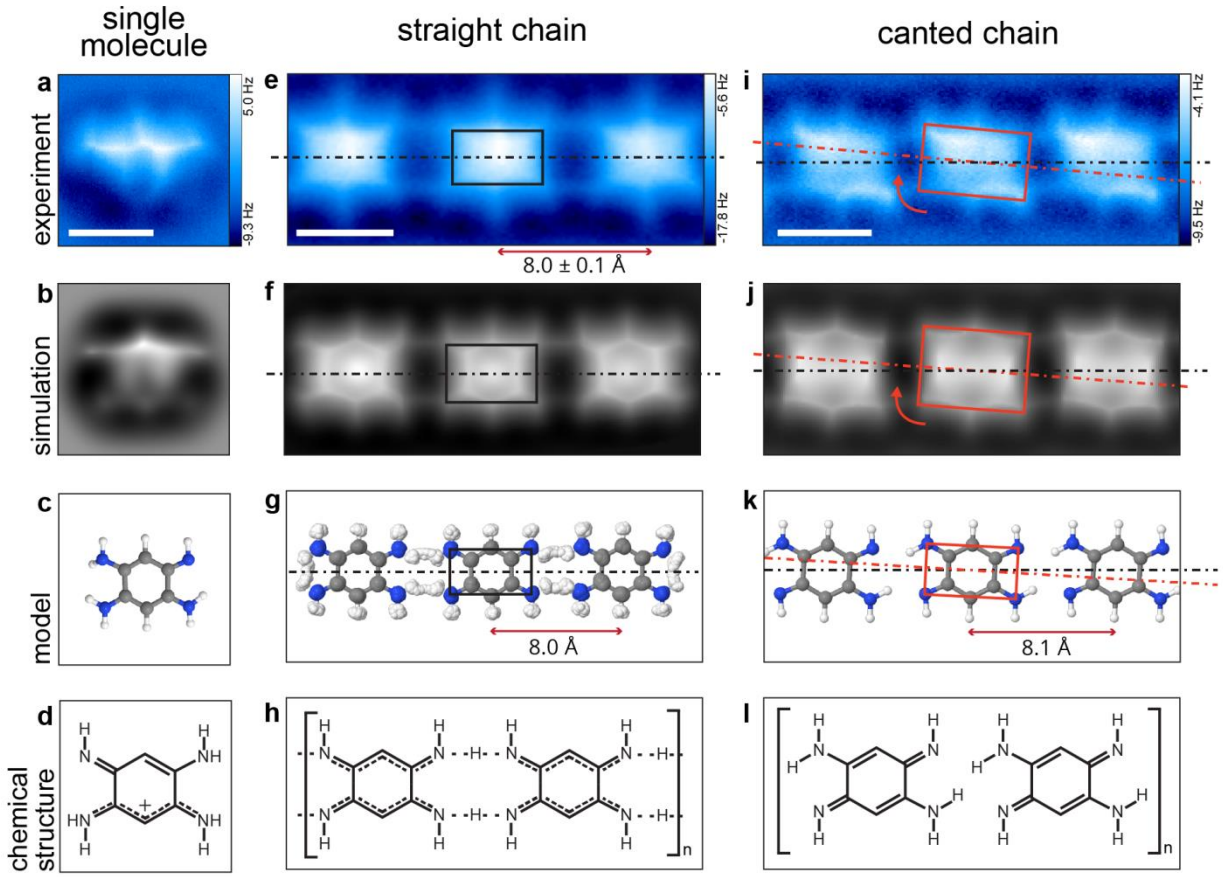

Figure 3: Comparison between experimentally acquired high resolution AFM images of the observed molecular species and their respective simulated high resolution AFM images based on the calculated models (DFT, for c) and k)). a) - d) Single molecule with one additional proton, that impedes subsequent chain growth. e)- h) Hydrogen bonded symmetric chain with concerted proton tunneling. Molecular units are symmetric around the chain axis. Model (g) calculated by PIMD at the transition state. i)- l) Hydrogen bonded canted chain (no proton tunneling). Molecules are canted with respect to the main axis and distinct contrast difference between imine and amine groups is visible (All scale bars are 500 pm).

A classical total energy DFT calculation of a molecular DABQDI chain assembled by hydrogen bonds (Fig. 3k, l) provides relatively good agreement but with slightly larger distance between two adjacent molecules (8.12 Å), further disfavoring the dative hypothesis. However, molecules in such chains are canted with respect to the main chain axis in order to decrease the energy by aiming the hydrogens participating in the hydrogen bond toward their respective nitrogen atoms. This is in contrast with the experimentally observed symmetric chain structure where all the molecular units are symmetric around the main axis (see Fig. 3e and Supplementary Fig.6a). We resolved this inconsistency by using Path Integral Molecular Dynamics (PIMD) simulations (details later) which account for NQEs (corresponding atomic structure shown in Fig. 3g). The calculated intermolecular distance using average atomic positions of PIMD calculations, 8.03 Å, fits very well to the experimental value (8.0 ± 0.1 Å). Moreover, the corresponding simulated AFM image (Fig. 3f) shows a highly symmetric arrangement caused by slight rearrangement of the positions of hydrogen and nitrogen atoms driven by the proton tunneling, which agrees with the experimental evidence.

On the other hand, the high-resolution AFM images acquired on canted chains (see Fig. 3i and Supplementary Fig. 6b) match the AFM simulation (Fig. 3j) of the canted structure predicted by the total energy DFT simulations (Fig. 3k). This indicates that in the canted chains the molecular units are frozen in one of the two possible configurations with lower energy due to an external constraint, while the symmetric chains are a superposition of the two degenerate electronic states that is driven by proton tunneling between adjacent nitrogen atoms. One possible way to confirm the relevance of the proton tunneling would be to carry out the same experiment with molecules synthesized using six deuterium atoms. Unfortunately, performing the same experiment with deuterated DABQDI precursor proved to be unfeasible, mainly due to its poor stability (discussed in the Supplementary Information).

To overcome this experimental limitation, we have performed PIMD simulations in order to elucidate the importance of NQEs and their impact on the structural properties of the molecular chains. We analyzed the results obtained from QM/MM (Quantum Mechanics/Molecular Mechanics) simulations[31] at different temperatures in which the quinone molecules were

included in the QM region and the metallic surface is in the classical region. Figure 4a shows a free energy profile using our QM/MM (DFT) method treating all the nuclei as classical particles, and quantum (PIMD) simulations of the concerted proton transfer between amine and imine groups within the chain at 20 K and 10 K, showing significant differences with respect to the classical free-energy profile at 10 K. The height of the quantum free-energy profile at 20 K decreases by approximately half with respect to the classical barrier and it is further lowered at 10 K. Moreover, the shape of the barrier also changes significantly, showing double well character with a concave dip in the central part of the barrier at 10 K, see Fig. 4a. This demonstrates that the NQEs cause strong proton delocalization across the tunneling barrier, revealing the presence of deep proton tunneling, as shown in Fig. 4b.

According to the quantum simulations, the intermolecular distance between two nitrogen atoms (3.03 Å) decreases with respect to the classical case (3.12 Å), facilitating the proton transfer. Moreover, NQEs not only change the spatial redistribution of hydrogens but also the adjacent nitrogen atoms, creating the symmetric atomic arrangement as shown on Fig. 4c. This symmetric atomic arrangement not only explains the observed AFM contrast of the chains (see Fig. 3e), but also facilitates more direct interaction between proton and nitrogen atoms, which alongside with the shortening of N-N bonds enhances the electrostatic interaction[5]. These effects may partially explain the experimentally observed mechanical stability of the symmetric chains. In addition, PIMD simulations with deuterated DABQDI molecules showed a substantial increase of the activation barrier with only limited proton tunneling (see Supplementary Fig. 15a).

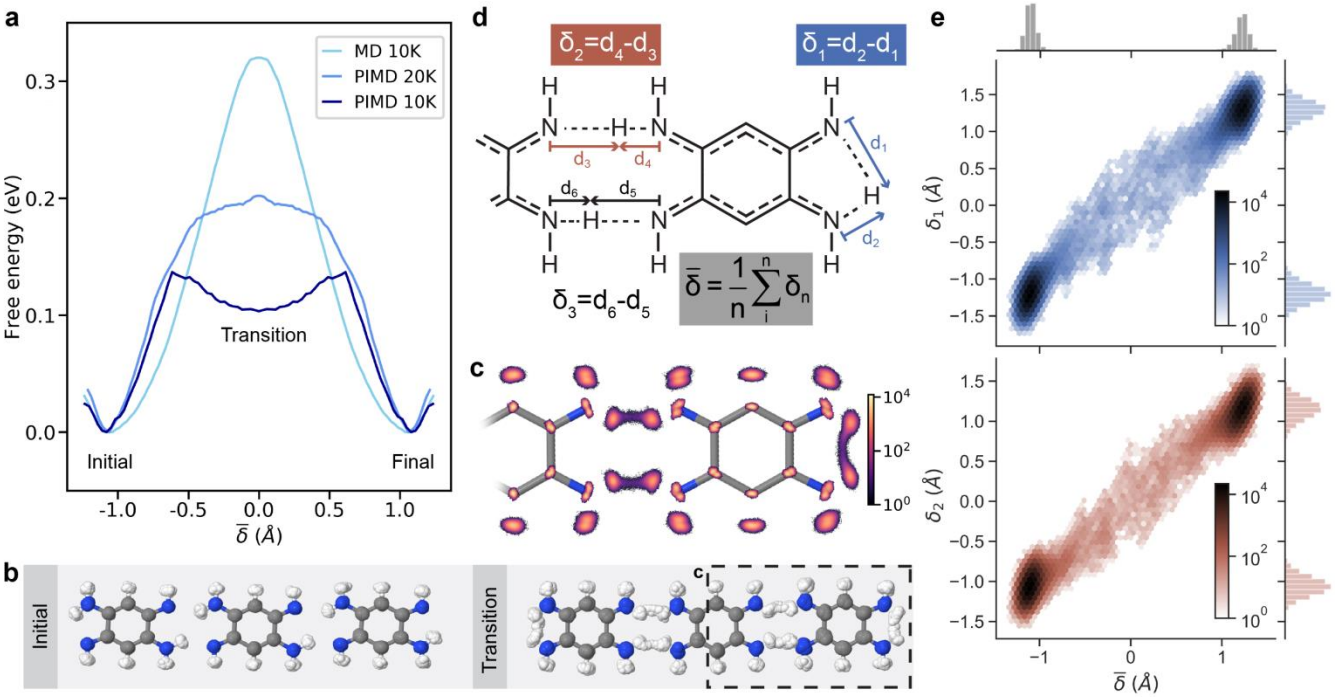

Figure 4: a) Free energy curve of the proton transfer calculated using classical MD at 10 K (cyan), Path Integral MD at 10 K (light blue) and Path Integral MD at 20 K (dark blue) with the average $\bar{\delta}$ of all hydrogen bonds as the reaction coordinate. b) PIMD structure for δ = -1 Å (initial) and δ = 0 Å (transition). PIMD structure for δ = 1 Å (final) is shown in Supplementary Fig. 15b c) 2D histogram of atomic density projected in the plane of the molecules at the transition state. d) Scheme of δ reaction coordinates. e) Correlation between the average delta and δ_2 (intra) and δ_1 (edge) with 2D distribution in logarithmic scale and marginal distributions in linear scale, respectively.

To understand a detailed mechanism of the proton tunneling process, we analyzed the correlation between positions of individual protons during the tunneling transfer. Figure 4e shows the spatial distribution of δ-reaction coordinates of two selected hydrogen bonds against the average δ-coordinate of all the hydrogen bonds in the chain (for the definition of δ-reaction coordinates see Fig. 4d). The δ-coordinate distribution plots show two well-localized peaks, which correspond to the two isomeric π-conjugations. The particular diagonal position of the distribution peaks reveals the concerted motion of all the protons during the tunneling process. This concerted motion can be rationalized as a preservation of the appropriate π-conjugation of the systems, which would be violated by an asynchronous proton transfer that would consequently increase the total energy of the system. In contrast, pure proton transfer would again violate the π-conjugation, *i.e.* alternation of single and double bonds. Thus, proton transfer has to be accompanied by electronic rearrangement, and we can interpret the process as proton-coupled electron transfer[32] introducing

a strong coupling between the electronic and vibrational proton degrees of freedom. This can explain why our adiabatic DFT and PIMD simulations are not able to reproduce the appearance of electronic in-gap end states, as discussed next.

From this perspective, the ground state of the chain should be viewed as a linear combination of two isomeric π-conjugations, which may effectively lead to the delocalization of π electrons over the chain. We note that the symmetric chains are characterized by the presence of bright spots at their ends, visible in STM imaging (Fig. 1b). To understand the origin of the bright spots, we performed scanning tunneling spectroscopy (STS; see Experimental Section) combined with high-resolution AFM imaging. This allows us to unambiguously correlate the chemical and electronic structure of the chain ends. STS spectra revealing the electronic structure of the end state are shown in Fig. 5a) for the positions indicated in Fig. 5b). Similar to the chain interior, the AFM image (Fig. 5b) shows a highly symmetric contrast supporting the presence of proton tunneling between two terminal nitrogen atoms. Figure 5d shows 1D STS spectroscopies taken along the central symmetry axis of the chain end (red dashed line in Fig. 5c, see also Supplementary Fig. 8), revealing the presence of an in-gap state tightly localized around the terminating molecule unit.

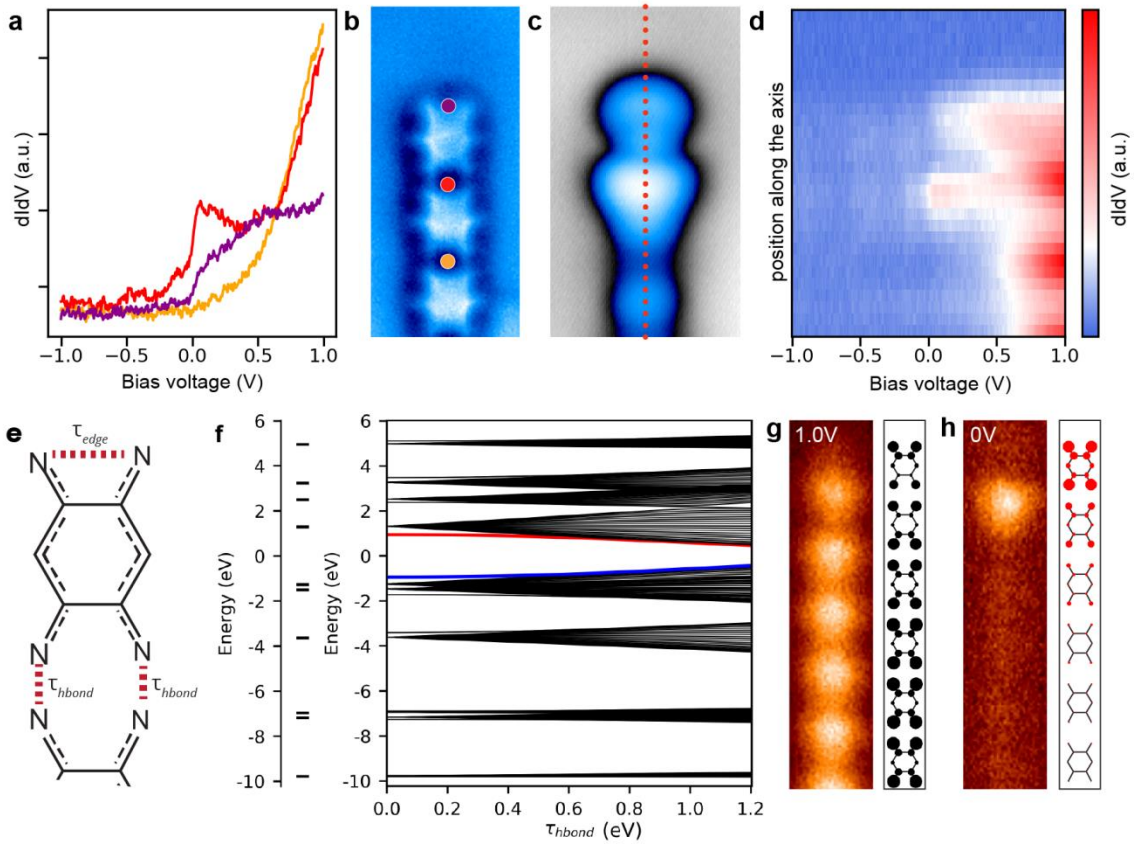

Figure 5*:* a) Selected STS spectra, taken at positions marked in b), showing the presence of the in gap electronic state. b) Representative experimental high resolution AFM image of the chain end. c) Representative experimental STM image of the chain end. (30mV, 10pA) d) Map of STS spectra taken along the chain axis at positions indicated in c) showing the spatial localization of the end state around the terminating molecular unit. (open loop - setpoint 1V, 80pA at position marked by the red dot in b)) e) Definition of coupling parameters τ_{hbond} and τ_{edge} in the tight-binding model of a molecular chain (only non-hydrogen atoms are shown as they are the sole hosts of p_z orbitals). f). The electronic spectra of single-molecule (left) and molecular chain (right, model composed of 20 molecules) as function of parameter τ_{hbond} (τ_{edge} = 0.9 eV). In-gap states highlighted in red and blue. g), h) Spatially-resolved differential conductance maps (left) acquired above the last six molecules of a straight chain at 1V and 0V respectively demonstrate the localization of the in-gap state. Density of states of the tight-binding model projected to every atom (right) for a sum of ten delocalized bulk-like states (DS, black) and the in-gap state (ES, orange). For a better comparison with the experimental images, only the last six molecules are shown.

The end-state is centered at 50 meV above the Fermi level. For the sake of clarity, selected spectra from spatial coordinates indicated in Fig. 5b are shown in Fig. 5a. This state only appears on the symmetric chain termination, remaining completely absent in the case of canted chains (Fig. 2 a, b).Thus, we attribute the appearance of the end-states (ESs) in the symmetric chains to the concerted proton tunneling motion, which allows the π-electron system to be effectively delocalized across the whole chain.

To understand the origin of the in-gap ESs, we analyzed the electronic structure of a tight-binding Hamiltonian mapping π-

conjugated electrons of the chain (for detailed description see Supplementary Information) as illustrated in Fig. 5e. First, we extracted tight-binding parameters representing π-electrons of an isolated molecule from our local basis DFT calculations[33] using the Löwdin transformation of exclusively p_z-orbitals (the electronic spectrum of single molecule is shown in Fig. 5f, left). We also introduced an intermolecular hopping τ_{hbond} between molecular units to the Hamiltonian (Fig. 5e), which in the case of classical H-bonds is much smaller (τ_{hbond} < 0.1eV) than the hopping corresponding to covalent double or single bonds. Consequently, the electronic structure of a chain consisting of only weakly electronically coupled molecular units remains very similar to the single molecule case with only a slight broadening of the molecular levels into bands (see Fig. 5f). On the other hand, the presence of concerted proton tunneling with its strong proton-coupled electron transfer, enhances the electronic coupling of the π-electrons in the system. To consider these effects we introduced an extra hopping τ_{edge} between two nitrogen atoms at the edges of the chain, shown on Fig. 5e. We have analysed the influence of the parameters τ_{hbond} and τ_{edge} on the electronic spectrum of this model Hamiltonian. For certain values of the hopping parameters τ_{hbond} and τ_{edge} corresponding to weak covalent bonds (slightly weaker than intramolecular covalent bonds formed by π-electrons of carbon and nitrogen atoms), we find in-gap states (the electronic spectra shown in Fig. 5f, with in-gap states highlighted by colors) spatially localized at the edges of the chain (Fig. 5h right) in contrast to the bulk-like states that are delocalized over the whole chain length (Fig. 5g right). Although constant height differential conductance map in Fig. 5h fails to distinctly show the presence of the in-gap states at the terminal N groups, it is worth noting, that the line spectra shown in Fig. 5d shows signal on both the inner and outer sides of the terminating molecular unit (seen also in Fig. 5a). The in-gap state localization at the chain termini can be better seen in the differential conductance map taken in constant current mode (see Supplementary Fig. 21). Note that the enhancement of the intermolecular hopping τ_{hbond} causes a reduction of the band gap of the straight chains relative to canted, which is in good agreement with STS measurements, see Supplementary Fig. 9. In this way the experimental observation of the ESs and the renormalization of the band gap provides additional support to the enhanced intermolecular interaction picture, which underlies the large mechanical stability of the chains observed experimentally.

Conclusion

Our results make a direct connection between concerted proton tunneling and the two signal characteristics of the symmetric chains: their enhanced mechanical stability, and the appearance of in-gap end-states. We demonstrate that NQEs can cause the emergence of distinct electronic states at the Fermi level due to strong electron-proton coupling, which leads to the delocalization of π-electrons within the molecular chain. These phenomena are relevant to the ingredients used to establish the high-temperature superconducting state recently observed in high-pressure hydrates,[34,35] and it indicates that the strength of hydrogen bonds may be enhanced close to covalency[36] due to NQEs. We believe that these findings will stimulate further investigation of nuclear quantum phenomena including a search for similar supramolecular systems beyond 1D where concerted proton motion and enhanced proton-coupled electron transfer strongly affect their collective mechanical and electronic properties.

Methods

Chain growth

The precursor molecule 2,5-diamino-1,4-benzoquinonediimines (DABQDI) was synthesized *via* the procedure described in the literature.[37] Atomically clean Au(111) was prepared by repeated Argon ion (Ar^+) sputtering/annealing cycles. Molecules were sublimed from a home-built evaporator with tantalum pocket onto the clean Au(111). To form **the straight chains**, three steps were followed: i) deposition of the DABQDI molecular precursor (crucible temperature 90-100°C) into the microscope head on a cold sample (5 K), ii) transfer of the sample out of the microscope head to the microscope chamber, where the sample was kept for 60 minutes on the wobble stick until it warmed up almost to the room temperature, iii) transfer of the sample back to the microscope head (5 K). To form **the canted chains**, molecules were evaporated in the preparation chamber (crucible temperature 90-120°C) onto a sample thermalized to 20-60°C before being immediately transferred to the microscope head. For more details please see the discussion in the Supplementary Information.

STM/AFM measurements

All experiments were performed in commercial ultrahigh vacuum (UHV) low-temperature microscopes with combined STM/AFM capabilities (Specs-JT Kolibri: PtIr tip, f_0 = 1 MHz, Q = 120 k, K = 540 kN/m and Createc-qPlus: PtIr tip, f_0 = 30 kHz, Q = 50k, K = 1.8 kN/m). To manipulate the chains, the metallic tip was approached to the chain end at V_{bias} = 5 mV until a characteristic, abrupt change in the current channel was observed. To achieve sub-molecular resolution, the tip apex was functionalized with a CO molecule lifted from the Au(111) substrate.[16] All STS data were acquired in constant height mode (open feedback loop) using the lock-in technique (Nanonis internal) with a bias modulation amplitude of 5 mV and frequency 932 Hz. Prior to STS data acquisition, the tips were calibrated with reference to the Au(111) Shockley surface state.

DFT Calculations

Density functional theory (DFT) calculations were performed using the FHI-AIMS code[38] within exchange-correlation functional B3LYP[39,40] to describe the electronic properties of the gas-phase DABQDI molecule and of its protonated form adsorbed on the Au(111) substrate using a 6x6 unit cell. In all the calculations, we employed the tight settings for the atomic basic sets. The atomic structures were thoroughly relaxed until the Hellman-Feynman forces were smaller than 10^{-3} eVÅ^{-1}. The relaxed structures were found by exploring different initial conditions and selecting the one with lowest potential energy. We have used the Tkatchenko-Scheffler correction[41] to include van der Waals interactions in the calculations. Only the Γ-point was used for integration in the Brillouin zone.

PIMD calculations

All the simulations were performed with 3 quinone molecules in local orbital DFT with local basis set Fireball code;[33] the surface was simulated using the interface forcefield.[42] DFT Fireball calculations used the BLYP exchange-correlation functional[39,43] with D3 corrections.[44] Classical MD was performed using the QM/MM method Fireball/Amber[31], while PIMD was performed using the i-PI software[45] with QM/MM interactions calculated by Fireball and LAMMPS.[46] We have used 512 PIMD replicas at 20 K and 1024 replicas at 10 K. To see the convergence with the number of replicas, see the Supplementary Information.

For the PIMD QM/MM simulation, an initial minimization of 10000 steps was performed followed by a classical QM/MM of 20 000 steps with a time step of 0.5 fs. For the PIMD we started with the results of the classical QM/MM and performed 20 000 steps with a time step of 0.25 fs.To obtain the free energy profile we performed umbrella sampling with the bias applied to the reaction coordinate profile was generated using the WHAM method[47] with 5000 steps in each window and a bias force of 200 kcal/mol on the reaction coordinate.

AFM simulations

The AFM images were calculated using the probe particle model.[48] The parameters of the tip were chosen to mimic a CO-tip, using a quadrupole charge moment of -0.1 e. A^{o2} ,[49] and the lateral stiffness of the CO molecule set to 0.25 Nm^{-1}. The electrostatic interaction was described in the AFM calculations using the potential calculated by DFT. To simulate the probe dynamics we used typical values of a qPlus sensor, oscillation amplitude A = 100 pm, sensor stiffness k = 3600 N/m and eigenfrequency f_0 = 30 kHz. The simulated AFM image, shown in Fig. 3f, is calculated as an average of AFM images of each replica of the PIMD simulations at 10 K.

ASSOCIATED CONTENT

Supplementary Information: Analysis of single molecules on a gold surface; Arguments to exclude metal-organic Au-DABQDI as the symmetric chains; Supporting arguments to exclude other possible scenarios; Notes on the sample preparation; STS of the end states with different metallic tips; STS comparison of canted and straight chains; The experiment with deuterated DABQDI precursors; Comparison of FHI-AIMS and Fireball DFT methods; Convergence based on the number of replicas in PIMD calculations at different temperatures; Free energy calculations; Analysis of the concerted motion of protons; Tight-Binding model on the molecular chain.

This material is available free of charge *via* the Internet at: https://pubs.acs.org/doi/10.1021/acsnano.1c02572

The manuscript has been previously submitted to the preprint server.[50]

AUTHOR INFORMATION

Corresponding Author

* Correspondence to:
Olivier Siri: olivier.siri@univ-amu.fr
Pavel Jelinek: jelinekp@fzu.cz

Author Contributions

P.J. and O.S. conceived the project and designed the experiments. A. C., J. H., V.M. S. and M. Š. performed and analyzed the SPM experiments. S. P. and O. S. synthesized organic molecules. J.I.M., D.S., S.I.E., K.V. and P.J. performed tight bonding modelling, P.M. performed DFT and AFM calculations, J.I.M., O.M. performed PIMD calculations. J.I.M., D.S., S.I.E., K.V, O.M. and P.J interpreted theoretical results and underlying mechanism. All authors discussed the results, co-wrote and commented on the manuscript.

[†]Aleš Cahlík, Jack Hellerstedt, Jesus I. Mendieta-Moreno contributed equally.

ACKNOWLEDGMENT

O.Siri thanks the Centre National de la Recherche Scientifique (CNRS) and the Ministère de la Recherche et des Nouvelles Technologies. This work was supported by the Czech Science Foundation (Reg. No. 18-09914 S, 20-13692X), We acknowledge CzechNanoLab Research Infrastructure supported by MEYS CR (LM2018110). P.Jelinek acknowledges support from Praemium Academie of the CAS. O.Marsalek was supported by the Primus16/SCI/27/247019 grant from Charles University. Computational resources were provided by the CESNET LM2015042 and the CERIT Scientific Cloud LM2015085, provided under the programme "Projects of Large Research, Development, and Innovations Infrastructures".

REFERENCES

1. Benoit, M., Marx, D. & Parrinello, M. Tunnelling and Zero-Point Motion in High-Pressure Ice. *Nature.* **1998**, *392*, 258–261.
2. Horiuchi, S., Tokunaga,Y., Giovannetti, G., Picozzi, S., Itoh,H., Shimano,R., Kumai, R., Tokura,Y. Above-Room-Temperature Ferroelectricity in a Single-Component Molecular Crystal. *Nature.* **2010**, *463*, 789–792 .
3. Frank, R. A. W., Titman, C. M., Pratap, J. V., Luisi, B. F., Perham, R. N. A Molecular Switch and Proton Wire Synchronize the Active Sites in Thiamine Enzymes. *Science* **2004**, *306*, 872–876.
4. Salna, B., Benabbas, A., Sage, J. T., Van Thor, J., Champion, P. M. Wide-Dynamic-Range Kinetic Investigations of Deep Proton Tunnelling in Proteins. *Nat. Chem.* **2016**, *8*, 874–880.
5. Li, X. Z., Walker, B., Michaelides, A. Quantum Nature of the Hydrogen Bond. *Proc. Natl. Acad. Sci. U. S. A.* **2011**, *108*, 6369–6373 .
6. Guo, J., Lü,J.-T., Feng, Y., Chen,J., Peng,J., Lin,Z., Meng,X., Wang,Z., Li, X.-Z., Wang, E.-G., Jiang, Y.Nuclear Quantum Effects of Hydrogen Bonds Probed by Tip-Enhanced Inelastic Electron Tunneling. *Science.* **2016**, *352*, 321–325.
7. Wang, L., Fried, S. D., Boxer, S. G., Markland, T. E. Quantum Delocalization of Protons in the Hydrogen-Bond Network of an Enzyme Active Site. *Proc. Natl. Acad. Sci. U. S. A.* **2014**, *111*, 18454–18459.
8. Bove, L. E., Klotz, S., Paciaroni, A.,Sacchetti, F. Anomalous Proton Dynamics in Ice at Low Temperatures. *Phys. Rev. Lett.* **2009**, *103*, 165901.

9. Lin, L., Morrone, J. A.,Car, R. Correlated Tunneling in Hydrogen Bonds. *J. Stat. Phys.* **2011**, *145*, 365–384.

10. Drechsel-Grau, C., Marx, D. Quantum Simulation of Collective Proton Tunneling in Hexagonal Ice Crystals. *Phys. Rev. Lett.* **2014**, *112*, 148302.

11. Liljeroth, P., Repp, J., Meyer,G. Current-Induced Hydrogen Tautomerization and Conductance Switching of Naphthalocyanine Molecules. *Science*. **2007**, *317*, 1203-1206.

12. Kumagai, T., Hanke, F., Gawinkowski, S., Sharp, J., Kotsis, K., Waluk, J., Persson, M., Grill, L. Controlling Intramolecular Hydrogen Transfer in a Porphycene Molecule with Single Atoms or Molecules Located Nearby. *Nature Chemistry.* **2014***, 6*, 41–46.

13. Ladenthin, J. N. , Frederiksen, T. , Persson, M. , Sharp, J. C. , Gawinkowski, S. , Waluk, J.,Kumagai, T.Force-Induced Tautomerization in a Single Molecule. *Nature Chemistry.* **2016***, 8*, 935.

14. Böckmann, H., Liu, S., Mielke, J., Gawinkowski, S., Waluk, J., Grill, L., Wolf, M.,Kumagai, T. Direct Observation of Photoinduced Tautomerization in Single Molecules at a Metal Surface. *Nano Lett.* **2016** *16,* 1034–1041.

15. Litman, Y., Richardson, J. O., Kumagai, T.,Rossi, M. Elucidating the Nuclear Quantum Dynamics of Intramolecular Double Hydrogen Transfer in Porphycene. *J. Am. Chem. Soc.***2019***, 141*,2526–2534.

16. Gross, L., Mohn,F., Moll,N., Liljeroth, P., Meyer, G. The Chemical Structure of a Molecule Resolved by Atomic Force Microscopy. *Science*. **2009,***325*, 1110–1114.

17. Jelinek, P. High Resolution SPM Imaging of Organic Molecules with Functionalized Tips. *J. Phys. Condens. Matter* **2017**, *29*, 343002.

18. Meng, X., Guo,J., Peng,J., Chen,J., Wang,Z., Shi,J.-R., Li,X.-Z., Wang,E.-G., Jiang, Y.Direct Visualization of Concerted Proton Tunnelling in a Water Nanocluster. *Nat. Phys.* **2015**, *11*, 235–239.

19. Pascal, S.,Siri, O. Benzoquinonediimine Ligands: Synthesis, Coordination Chemistry and Properties. *Coord. Chem. Rev.* **2017**, *350*, 178–195.

20. Siri, O., Braunstein, P., Rohmer, M. M., Bénard, M., Welter, R. Novel 'Potentially Antiaromatic', Acidichromic Quinonediimines with Tunable Delocalization of Their 6π-Electron Subunits. *J. Am. Chem. Soc.* **2003**, *125*, 13793–13803 .

21. Dähne, S. Leupold, D. Coupling Principles in Organic Dyes. *Angew. Chemie Int. Ed. English*. **1966**,*5*, 984–993 .

22. Rumpel, H. & Limbach, H. H. NMR Study of Kinetic HH/HD/DD Isotope, Solvent, and Solid-State Effects on the Double Proton Transfer in Azophenine. *J. Am. Chem. Soc.* **1989**, *111*, 5429–5441.

23. Nietzki, R.,Hagenbach, E. Ueber Tetramidobenzol und Seine Derivate. *Berichte der Dtsch. Chem. Gesellschaft*. **1887**,*20*, 328–338.

24. Griffiths, D. J., Schroeter, D. F. *Introduction to Quantum Mechanics*. (Cambridge University Press, Cambridge, 2018). doi:10.1017/9781316995433

25. Gross, L., Mohn,F., Moll,N., Schuler,B., Criado,A., Guitián,E., Peña,D., Gourdon,A., Meyer, G. Bond-Order Discrimination by Atomic Force Microscopy. *Science*. **2012**, *337*, 1326–1329.

26. de Oteyza, D. G., Gorman, P., Chen, Y.-C., Wickenburg,S., Riss,A., Mowbray. D.J., Etkin,G., Pedramrazi,Z., Tsai,H.-Z., Rubio,A., Crommie, M.F., Fischer,F.R. Direct Imaging of Covalent Bond Structure in Single-Molecule Chemical Reactions. *Science.* **2013**, *340*, 1434–1437 .

27. Emmrich, M., Emmrich, M., Huber, F., Pielmeier, F., Welker, J., Hofmann, T., Schneiderbauer, M., Meuer, D., Polesya,S., Mankovsky,S., Ködderitzsch,D., Ebert, H., Giessibl, F.J., Subatomic Resolution Force Microscopy Reveals Internal Structure and Adsorption Sites of Small Iron Clusters. *Science.* **2015**, *348*, 308–311 (2.

28. Hapala, P., Švec,M., Stetsovych,O., van der Heijden, N.J., Ondráček, M., van der Lit,J., Mutombo,P., Swart,I., Jelínek,P. Mapping the Electrostatic Force Field of Single Molecules from High-Resolution Scanning Probe Images. *Nat. Commun.* **2016**, *7*, 11560 .

29. de la Torre, B., Švec,M., Hapala,P., Redondo,J., Krejčí,O., Lo,R., Manna,D., Sarmah,A., Nachtigallová,D., Tuček,J., Błoński,P., Otyepka,M., Zbořil,R., Hobza,P., Jelínek,P. Non-Covalent Control of Spin-State in Metal-Organic Complex by Positioning on N-Doped Graphene. *Nat. Commun.* **2018**, *9*, 2831.

30. Santhini, V. M., Wackerlin,C., Cahlik, A., Ondracek,M., Pascal,S., Matej,A., Stetsovych,O., Mutombo, P., Lazr, P., Siri, O., Jelinek, P. 1D Coordination π–d Conjugated Polymers with Distinct Structures Defined by the Choice of the Transition Metal: Towards a New Class of Antiaromatic Macrocycles. *Angew. Chemie Int. Ed.* **2021**, *60*, 439–445.

31. Mendieta-Moreno, J. I., Walker, R.C., Lewis, J.P., Gómez-Puertas, P., Mendieta, J., Ortega, J. Fireball / Amber: An Efficient Local-Orbital DFT QM/MM Method for Biomolecular Systems. *J. Chem. Theory Comput.* **2014**, *10*, 2185–2193.

32. Huynh, M. H. V., Meyer, T. J. Proton-Coupled Electron Transfer. *Chem. Rev.* **2007**, *107*, 5004–5064.

33. Lewis, J. P., Jelínek,P., Ortega, J., Demkov, A.A., Trabada, D.G., Haycock, B., Wang, H., Adams, G., Tomfohr, J.K., Abad, E., Wang, H., Drabold, D.A. Advances and Applications in the FIREBALL *ab Initio* Tight-Binding Molecular-Dynamics Formalism. *Phys. Status Solidi Basic Res.* **2011**, *248*, 1989–2007 .

34. Drozdov, A. P., Eremets, M. I., Troyan, I. A., Ksenofontov, V., Shylin, S. I. Conventional Superconductivity at 203 Kelvin at High Pressures in the Sulfur Hydride System. *Nature.* **2015***, 525*, 73–76.

35. Drozdov, A. P., Kong, P. P., Minkov, V. S., Besedin, S. P., Kuzovnikov, M. A., Mozaffari, S., Balicas, L., Balakirev, F. F., Graf, D. E., Prakapenka, V. B., Greenberg, E., Knyazev, D. A., Tkacz, M., Eremets, M. I. Superconductivity at 250 K in Lanthanum Hydride under High Pressures. *Nature.* **2019***, 569*, 528–531 .

36. Grabowski, S. J. What Is the Covalency of Hydrogen Bonding? *Chem. Rev*. **2011**, *111*, 2597–2625.

37. Audi, H., Chen, Z., Charaf-Eddin, A., D'Aléo, A., Canard, G., Jacquemin, D., Siri, O. Extendable Nickel Complex Tapes That Reach NIR Absorptions. *Chem. Commun.* **2014**, *50*, 15140–15143 .

38. Blum, V., Gehrke, R., Hanke, F., Havu, P., Havu, V., Ren, X.,Reuter, K., Scheffler, M. A*b Initio* Molecular Simulations with Numeric Atom-Centered Orbitals. *Comput. Phys. Commun.* **2009**, *180*, 2175–2196.

39. Becke, A. D. A New Mixing of Hartree-Fock and Local Density-Functional Theories. *J. Chem. Phys.* **1993**, *98*, 1372–1377 .

40. Stephens, P. J., Devlin, F. J., Chabalowski, C. F., Frisch, M. J. A*b Initio* Calculation of Vibrational Absorption and Circular Dichroism Spectra Using Density Functional Force Fields. *J. Phys. Chem.* **1994**, *98*, 11623–11627 .

41. Tkatchenko, A., Scheffler, M. Accurate Molecular van der Waals Interactions from Ground-State Electron Density and Free-Atom Reference Data. *Phys. Rev. Lett.* **2009**, *102*, 073005.

42. Heinz, H., Lin, T. J., Kishore Mishra, R.,Emami, F. S. Thermodynamically Consistent Force Fields for the Assembly of Inorganic, Organic, and Biological Nanostructures: The INTERFACE Force Field. *Langmuir.* **2013**, *29*, 1754–1765 .

43. Lee, C., Yang, W.,Parr, R. G. Development of the Colle-Salvetti Correlation-Energy Formula into a Functional of the Electron Density. *Phys. Rev. B.* **1988***, 37*, 785–789.

44. Grimme, S., Ehrlich, S.,Goerigk, L. Effect of the Damping Function in Dispersion Corrected Density Functional Theory. *J. Comput. Chem.* **2011**, *32*, 1456–1465 .

45.Kapil, V., Rossi, M. Marsalek, O., Petraglia, R., Litman, Y., Spura, T., Cheng, B., Cuzzocrea, A., Meißner, R.H., Wilkins, D.M., Helfrecht, B.A., Juda, P., Bienvenue, S.P., Fang, W., Kessler, J., Poltavsky, I., Vandenbrande,S., Wieme, J., Corminboeuf, C., Kühne, T.D. i-PI 2.0: A Universal Force Engine for Advanced Molecular Simulations. *Comput. Phys. Commun.* **2019**, *236*, 214–223.

46. Plimpton, S. Fast Parallel Algorithms for Short-Range Molecular Dynamics. *J. Comput. Phys.* **1995**, *117*, 1–19 .

47. Kumar, S., Rosenberg, J. M., Bouzida, D., Swendsen, R. H.,Kollman, P. A. The Weighted Histogram Analysis Method for Free-Energy Calculations on Biomolecules. I. The Method. *J. Comput. Chem.***1992,** *13*, 1011–1021 .

48. Hapala, P., Kichin,G., Wagner,C., Tautz, F.S., Temirov, R., Jelínek, P. Mechanism of High-Resolution STM/AFM Imaging with Functionalized Tips. *Phys. Rev. B*. **2014**, *90*, 085421 .

49. Peng, J., Guo, J., Hapala, P., Cao, D., Ma, R., Cheng, B., Xu, L., Ondráček, M., Jelínek, P., Wang, E., & Jiang, Y. Weakly Perturbative Imaging of Interfacial Water with Submolecular Resolution by Atomic Force Microscopy. *Nat. Commun.* **2018**, *9*, 122 .

50. Cahlík, A., Hellerstedt, J., Mendieta-Moreno, J. I., Švec, M., Santhini, V. M., Pascal, S., Soler-Polo, D., Erlingsson, S. I., Výborný, K., Mutombo, P., Marsalek, O., Siri, O., & Jelínek, P. Significance of Nuclear Quantum Effects in Hydrogen Bonded Molecular Chains. 2020, 2007.14657. arXiv. https://arxiv.org/abs/2007.14657 (accessed May 14, 2021).